Neurobiology of Aging 94 (2020) 89–100

Contents lists available at ScienceDirect

Neurobiology of Aging

journal homepage: www.elsevier.com/locate/neuaging

Somatosensory area 3b is selectively unaffected in corticobasal syndrome: combining MRI and histology

Lars Dinkelbach[a,b], Martin Südmeyer[a,g], Christian Johannes Hartmann[a,c], Sigrun Roeber[d], Thomas Arzberger[d,e], Jörg Felsberg[f], Stefano Ferrea[a], Alexia-Sabine Moldovan[a,c], Katrin Amunts[h,i,j], Alfons Schnitzler[a,c], Svenja Caspers[b,h,i,*]

[a] Institute of Clinical Neuroscience and Medical Psychology, Medical Faculty, Heinrich Heine University of Düsseldorf, Düsseldorf, Germany
[b] Institute for Anatomy I, Medical Faculty, Heinrich Heine University of Düsseldorf, Düsseldorf, Germany
[c] Department of Neurology, Heinrich Heine University of Düsseldorf, Düsseldorf, Germany
[d] Center for Neuropathology and Prion Research, Ludwig Maximilian University of Munich, Munich, Germany
[e] Department of Psychiatry and Psychotherapy, University Hospital, LMU Munich, Munich, Germany
[f] Department of Neuropathology, Heinrich Heine University of Düsseldorf, Düsseldorf, Germany
[g] Department of Neurology, Ernst von Bergmann Klinikum, Potsdam, Germany
[h] Institute of Neuroscience and Medicine (INM-1), Research Centre Jülich, Jülich, Germany
[i] JARA-BRAIN, Jülich-Aachen Research Alliance, Research Centre Jülich, Jülich, Germany
[j] C. & O. Vogt Institute for Brain Research, Medical Faculty, Heinrich Heine University of Düsseldorf, Düsseldorf, Germany

ARTICLE INFO

Article history:
Received 15 November 2019
Received in revised form 4 April 2020
Accepted 14 May 2020
Available online 21 May 2020

Keywords:
Corticobasal syndrome
Atypical parkinsonism
Neurodegeneration
Neuroimaging
Biomarker

ABSTRACT

An increasing number of neuroimaging studies addressing patients with corticobasal syndrome use macroscopic definitions of brain regions. As a closer link to functionally relevant units, we aimed at identifying magnetic resonance–based atrophy patterns in regions defined by probability maps of cortical microstructure. For this purpose, three analyses were conducted: (1) Whole-brain cortical thickness was compared between 36 patients with corticobasal syndrome and 24 controls. A pattern of pericentral atrophy was found, covering primary motor area 4, premotor area 6, and primary somatosensory areas 1, 2, and 3a. Within the central region, only area 3b was without atrophy. (2) In 18 patients, longitudinal measures with follow-ups of up to 59 months (mean 21.3 ± 15.4) were analyzed. Areas 1, 2, and 6 showed significantly faster atrophy rates than primary somatosensory area 3b. (3) In an individual autopsy case, longitudinal in vivo morphometry and postmortem pathohistology were conducted. The rate of magnetic resonance–based atrophy was significantly correlated with tufted-astrocyte load in those cytoarchitectonically defined regions also seen in the group study, with area 3b being selectively unaffected.

1. Introduction

Corticobasal syndrome (CBS) refers to a rapidly progressive neurodegenerative Parkinsonian syndrome, characteristically consisting of asymmetric limb rigidity, dystonia, myocloni, and/or cortical sensory loss accompanied by higher cortical symptoms such as limb apraxia or alien limb phenomenon (Armstrong et al., 2013; Boeve et al., 2003). Initially, CBS was described as the typical presentation of corticobasal degeneration (CBD) (Rebeiz et al., 1968), but in the past two decades, multiple studies have shown that frequent underlying neuropathologies of CBS additionally include progressive supranuclear palsy (PSP) or Alzheimer's disease (AD) (Boeve et al., 1999; Josephs et al., 2006; Lee et al., 2011; Ling et al., 2010; Ouchi et al., 2014). Remarkably, CBD itself shows a heterogenous clinical presentation, whereas CBD-CBS was present in only 26%–68% of cases during patients' lifetimes (Alexander et al., 2014; Kertesz et al., 2005; Ling et al., 2010). As each of these neuropathological entities can have varying distributions leading to different clinical presentations, it has been proposed that clinical presentation is caused more by cortical and subcortical distribution of the underlying pathology than the pathologic entity itself (Dickson et al., 2010; Kouri et al., 2011; Tsuboi et al., 2005). In two studies, the pattern of atrophy in

* Corresponding author at: Institute for Anatomy I, Medical Faculty, Heinrich Heine University Düsseldorf, D-40225 Düsseldorf, Germany. Tel.: +49 211 8112681; fax: +49 211 81 116 15841.
E-mail address: svenja.caspers@hhu.de (S. Caspers).

0197-4580/
https://doi.org/10.1016/j.neurobiolaging.2020.05.009

patients with CBS was compared between pathohistologically proven CBS-AD, CBS-PSP, and CBS-CBD cases (Lee et al., 2011; Whitwell et al., 2010). Whereas the degree of atrophy differed between diseases, pericentral atrophy was found irrespective of the underlying pathology, making this the most probable morphologic substrate of CBS (Lee et al., 2011).

Several other studies used voxel-based morphometry of cortical and subcortical gray and white matter (Borroni et al., 2008; Boxer et al., 2006; Huey et al., 2009; Josephs et al., 2008; Lee et al., 2011; McMillan et al., 2016; Whitwell et al., 2010) or surface-based estimates of cortical thickness (Upadhyay et al., 2016) to describe the specific structural deviations underlying CBS in vivo. Consistently, a pattern of frontoparietal atrophy covering supplemental, premotor, and primary motor areas, primary somatosensory cortices, and the superior parietal cortex as well as striatal and thalamic atrophy was found when compared with healthy controls (Borroni et al., 2008; Boxer et al., 2006; Huey et al., 2009; Josephs et al., 2008; McMillan et al., 2016; Upadhyay et al., 2016; Whitwell et al., 2010). Longitudinally, a similar pattern of atrophy was described (Dutt et al., 2016; Südmeyer et al., 2012). A similar distribution of tau burden mainly affecting frontoparietal areas was found postmortem in PSP-CBS and CBD-CBS (Ling et al., 2016; Tsuboi et al., 2005). Recently, a direct link between tau burden in PSP and CBD and magnetic resonance imaging (MRI) atrophy within macroscopically defined regions was established (Spina et al., 2019), highlighting the suitability of MR-based morphometry for studying pathophysiology in vivo.

However, morphometric studies so far have focused on atrophy patterns of macroscopically defined regions, for example, lobes or gyri and sulci. Such definitions, however, fall short in capturing the functionally relevant units of the cortex, that is, cortical areas, which rarely follow macroscopic landmarks. This is also true for the sensorimotor cortex, where only the border between the motor and the sensory domains, but not within them or with external areas, are linked to the bottom of the central sulcus. The cortex can be microstructurally segmented into areas with differing cell compositions and distribution, that is, cytoarchitecture (Amunts and Zilles, 2015; Zilles and Amunts, 2010). Electrophysiological and imaging studies have shown that response patterns differ among cytoarchitectonically defined areas and therefore suggest that microstructure reflects functionality (de la Vega et al., 2016; Eickhoff et al., 2006, 2010; Genon et al., 2018; Iwamura et al., 1994; Merzenich et al., 1978). The availability of cytoarchitectonic maps as part of 3D human brain atlases means that atrophy can be described in MRI-based morphometric studies within functionally relevant units, and this thus provides a valuable approach to gain further insight into the pathophysiological mechanisms of neurodegenerative diseases (Schmitz et al., 2016; Südmeyer et al., 2012; Wang et al., 2015).

In CBS, only one longitudinal pilot trial consisting of six patients reported volume changes within regions defined by probability maps of cortical microstructure (Südmeyer et al., 2012). This analysis showed significant atrophy in primary motor area 4, premotor area 6, and primary somatosensory area 3a, while somatosensory areas 1, 2, and 3b were not involved. The finding of a differential affliction of functionally relevant areas within the somatosensory cortex is supported by the clinical phenotype of CBS, with stereognosis as one of its key features while primary tactile functions are usually preserved (Levin et al., 2016; Mahapatra et al., 2004). These preliminary findings and the clinical phenotype indicate a region-specific vulnerability of microstructurally defined cortical areas along the central sulcus, which is particularly addressed in the present study.

Here, we aim to (1) allocate the structural changes related to CBS with regard to probability maps of microstructurally defined, functionally relevant cortical areas and specific subcortical regions in comparison with healthy controls; (2) verify the cross-sectional findings longitudinally; and (3) directly link the longitudinal in vivo MRI-based measures of cortical thickness to the underlying histopathology within microstructurally defined cortical areas in one exemplary case of PSP-CBS.

2. Methods

2.1. Subjects

In this prospective mixed cross-sectional and longitudinal study, 36 patients with CBS and 24 age- and gender-matched healthy controls were recruited at the University Hospital of Düsseldorf. The groups did not differ regarding age (mean ± SD; patients: 65.6 ± 7.5; controls: 63.3 ± 8.1; t-test $p = 0.276$) or gender (female/male; patients: 25/11; controls: 16/8; chi-squared test $p = 0.821$). The diagnosis of CBS was consensually made by two movement disorder experts (AS and MS) after excluding other more probable diseases and based on a synopsis of clinical, imaging, and laboratory findings. All 36 patients fulfilled the Mayo Criteria for CBS (Boeve et al., 2003). Retrospectively, all patients fulfilled the Armstrong criteria for possible CBD and 26 (72.2%) patients for probable CBD over the course of the disease (Armstrong et al., 2013). A detailed summary of patients' characteristics is depicted in Table 1. For 18 patients and 18 healthy controls, longitudinal follow-ups were available. The healthy controls were matched one-to-one to patients and did not differ regarding age (mean ± SD in years; patients: 64.3 ± 6.7; controls: 63.5 ± 9.3, t-test $p = 0.775$) or gender (patients: 14 female, controls 12 female, chi-squared test $p = 0.457$). In total, 109 time points of 18 patients and 46 time points of 18 controls were recorded for the longitudinal analysis (mean ± SD; patients: number of follow-ups: 6.1 ± 3.9, range 2–16; time to last follow-up in months: 21.3 ± 15.4, range 6–59 months; controls: the number of follow-ups: 2.6 ± 0.5, range 2–3; time to last follow-up in months: 11.7 ± 3.4, range 6–23 months). To reduce the number of multiple comparisons, the longitudinal analyses focused on the clinically dominant brain hemisphere (i.e., contralateral to the clinically dominant body side) of the cortical and those subcortical regions with significant findings in the cross-sectional analysis. In healthy controls matched one-to-one to patients, the corresponding hemisphere for each case was chosen. A subset of the longitudinal data described here consisting of six patients was analyzed earlier using longitudinal voxel-based techniques (Südmeyer et al., 2012).

All patients and healthy controls were informed in detail about the nature of this study and gave written informed consent for their participation. The study was approved by the local ethics committee and was conducted in accordance with the Declaration of Helsinki.

2.2. Image acquisition and processing

Three-dimensional T1-weighted images with 1 mm isotropic voxel resolution (TR/TE 2300/2.98 ms; 256×256 matrix) were acquired on a 3 Tesla TIM-Trio MRI scanner (Siemens Medical Solutions; Erlangen, Germany). Raw data were visually checked for marked artifacts in the regions of interest (ROIs), without the need to exclude patients. The imaging data were processed in the cross-sectional and longitudinal pipeline of FreeSurfer 6.0.0 (https://surfer.nmr.mgh.harvard.edu/) (Dale et al., 1999; Fischl and Dale, 2000; Reuter et al., 2012). Skull-stripped and segmented images were visually checked for marked artifacts in the ROIs. Surfaces could not be reconstructed in the follow-up images of one patient (no. 19, see Table 1) because of image defects. Thus, this patient was included in the cross-sectional but not in the longitudinal analyses. In one subject (no. 35), segmentation was not plausible at 8 months

Table 1
Patient demographics and clinical characteristics

Patient	Sex	Age	Disease duration[b]	Side of onset	UPDRS	UPDRS initial lateralization[c]	UPDRS final lateralization[c]	Dystonia	Myoclonus	Apraxia[d]		Alien limb	Sensory deficit[e]	MMSE
1	f	73	1.8	Left	36	−7		-	-	++	15	++	++	28/30
2	f	55	7.4	Left	32	−5		++	++	-	36	-	-	28/30
3[a]	m	69	1.4	Left	21	−7	−10	-	++	++		-	+	26/30
4	f	66	1.8	Left	30	−6		++	++	++	12	++	++	22/30
5	f	75	2.3	Left	41	−11		++	++	++	8	++	++	24/30
6[a]	f	59	2.8	Right	21	7	7	++	++	-	37	-	-	30/30
7[a]	f	49	2.8	Left	34	−10	−10	+	++	+		++	+	28/30
8[a]	m	63	4.2	Left	21	−15	−11	++	-	-		-	+	30/30
9	m	60	1.6	Right	39	10		-	++	++	2	-	++	26/30
10[a]	f	72	0.8	Right	29	7	10	++	++	++	15	++	++	30/30
11[a]	f	63	3.3	Right	40	11	5	++	-	++	34	++	++	26/30
12	f	56	1.3	Right	29	2		++	-	++		-	-	29/30
13[a]	f	64	2.2	Right	21	5	4	-	++	++	30	-	++	29/30
14	m	64	2.4	Right	43	2		-	++	++		-	++	
15[a]	f	74	2.1	Left	32	−4	−2	-	-	++		+	-	29/30
16[a]	f	76	2.3	Right	12	3	6	-	++	++	35	-	++	29/30
17[a]	f	62	2.9	Right	19	8	0	+	++	++		++	++	30/30
18	m	66	2.4	Right	65	7		++	++	++	14	-	-	
19	m	76	2.4	Left	39	−8	−6	++	-	++		++	+	21/30
20	f	57	4.6	Left	22	−9		++	++	++	11	++	-	22/30
21	f	56	4.6	Right	30	7		++	-	++	5	-	++	25/30
22[a]	f	55	1.8	Right			5	++	-	++	22	-	-	27/30
23	f	62	1.3	Right	44	8		++	++	++	20	++	++	25/30
24	f	74	2.6	Left	35	−9		++	++	++		++	++	
25[a]	f	67	2.7	Left	42	−19	−11	++	-	+		-	++	
26[a]	f	68	1.3	Left			−9	++	++	++		-	++	26/30
27	f	77	3.8	Right	24	9		++	-	++	17	++	-	29/30
28[a]	f	66	1.2	Right	10	4	4	+	-	++	27	-	++	30/30
29	f	71	2.6	Left	35	−12		-	-	++		++	-	28/30
30	m	62	2.0	Left	67	−3		++	++	++		-	-	23/25
31	m	78	4.2	Left	30	−12		-	++	++	15	++	++	27/30
32[a]	f	66	1.1	Right	42	12	9	++	++	++	33	-	+	30/30
33[a]	m	62	3.3	Right	10	4	3	-	++	-	37	++	-	30/30
34[a]	f	56	1.6	Left	17	−5	−5	-	+	++	27	-	++	27/30
35[a]	m	66	1.0	Right	4	3	2	+	++	++		+	++	30/30
36	m	75	1.8	Left	26	−11		-	++	-	37	++	++	29/30
Mean ± SD		65.6 ± 7.5	2.5 ± 1.3		30.6 ± 13.8						22.2 ± 11.5			

Key: UPDRS, United Parkinson's Disease Rating Scale; MMSE, Mini-Mental State Examination; SD, standard deviation.
Patient characteristics at initial presentation. ++, present on initial clinical examination; +, clinical feature developed during the course of the disease; -, absent.

[a] Patients included in longitudinal analysis.

[b] Disease duration (onset of symptoms to the first study visit) in years.

[c] Lateralization of symptoms, calculated by the difference between the right and the left lateralized measures of the UPDRS. Negative values represent a lateralization of symptoms with more severe symptoms at the left and positive values a lateralization to the right side of the body. The initial lateralization presents the lateralization at the first time of imaging, the final lateralization presents the lateralization at the last available follow-up.

[d] Goldenberg's hand- and finger-position test for ideomotor apraxia (Goldenberg, 1995, 1996). In these tasks, patients are asked to imitate meaningless gestures consisting of either specific finger movements or the position of the whole hand in relation to the head. Both scales range from 0 – marked apraxia to 20 – unexceptional result. A score ≤17 in one of the tests was interpreted as clinically apparent apraxia. In the table, the sum of both tasks is shown, leading to a range from 0–40. However, apraxia tests were introduced during the course of the study and were therefore not available for all patients. In cases without apraxia tests, the description of apraxia as shown relied on nonstandardized clinical examinations.

[e] Impaired stereognosis or focal hypoesthesia.

of follow-up, and therefore, this follow-up was excluded from the analysis.

Whole-brain vertex-wise comparison of cortical thickness was conducted between baseline scans of 36 patients and 24 controls. To specifically identify the functionally relevant cortical units, probability maps of microstructurally defined cortical regions derived from the JuBrain Cytoarchitectonic Atlas (https://www.jubrain.fz-juelich.de) were used (Amunts and Zilles, 2015; Zilles and Amunts, 2010). For cortical ROIs, the cortical thickness within areas of the pericentral region, that is, the primary somatosensory cortex (areas 1, 2, 3a, 3b), primary motor cortex (area 4), and premotor cortex (area 6), were extracted (Geyer, 2004; Geyer et al., 1996, 1999, 2000). This strict focus on the pericentral regions was driven by our aim to focus on atrophy patterns, which can be found irrespective of the underlying pathology and thus provides a core feature of CBS [(Lee et al., 2011); see also Section 3 and Fig. 1]. For subcortical structures, the volumes of the brainstem, thalamus, amygdala, hippocampus, putamen, pallidum, caudate, and nucleus accumbens were extracted. For inferential statistics, the volumes of subcortical structures were corrected for the head size using the individual estimated total intracranial volumes (Buckner et al., 2004). For cross-sectional comparisons of the baseline scans of 36 patients with CBS and 24 controls, multiple t-tests were calculated. To analyze group effects in the longitudinal sample of 18 patients with CBS and 18 controls, multiple linear mixed models using group and time as well as their interactions as fixed effects and the cortical thickness/subcortical volume as dependent variable were calculated for each ROI using the restricted maximum likelihood method. To account for nonindependence due to repeated measures, time was included under the repeated statement with an autoregressive covariance structure, assuming that the correlation between measurements declines with longer intervals between time points. To account for the heterogeneity of baseline morphology, a random intercept was used. For subcortical structures, the intracranial volume was included as a covariate. In addition, a multiple linear mixed model using cortical regions and time as well as their interactions as fixed effects was calculated within patients to assess for differences in changes over time between cortical regions. The p-values of all cross-sectional and longitudinal end points were corrected for multiple comparisons using the Benjamini-Hochberg method to control the false discovery rate (Benjamini and Hochberg, 1995). False discovery rate–corrected p-values < 0.05 were considered statistically significant. Details of subject acquisition and image processing are described in Supplemental Material 1.

2.3. Histopathology

One 70-year-old patient with clinical CBS and neuropathologically defined PSP-CBS underwent two high-resolution structural MRI scans (voxel size 0.75 mm, at initial visit and at 26 months of follow-up) and consented to donate his brain tissue under the auspices of the "BrainNet" project of the Center for Neuropathology and Prion Research, University of Munich. The whole right hemisphere was embedded into paraffin and cut into serial coronal sections of 20 μm thickness. Each 240th section was stained for cell bodies using a modified silver stain (Merker, 1983). This enabled simultaneous optimal visualization of the relevant microstructural properties of the cortical areas (Amunts and Zilles, 2015) as well as of tufted astrocytes, the pathological hallmark and marker for degenerative processes in PSP (Togo and Dickson, 2002), which are known to particularly demask in silver staining methods (Dickson et al., 2010; Iwasaki et al., 2004). To assess the cortical burden of tufted astrocytes along the cortical ribbon within 1 × 1-mm-sized tiles, an observer-independent machine-based learning approach (Arganda-Carreras et al., 2017) was used. A comparison with manually quantified tufted astrocytes by an experienced neuropathologist (JF) and the automatically assessed burden with tufted astrocytes in 38 sections showed good consistency between both methods (Pearson's r = 0.855, $p < 0.001$, mean difference between automatic-manual = 11.3). A detailed description of the clinical and pathological phenotype as well as the histological preparation and machine-based learning approach can be found in Supplemental Material 1 and Supplemental Fig. 1.

3. Results

3.1. Cross-sectional differences in cortical thickness and subcortical volumes

When compared with healthy controls, surface-based whole-brain comparison of cortical thickness in baseline scans revealed a widespread pattern of bilateral pericentral atrophy in patients with CBS (see Fig. 1). Remarkably, a region on the caudal bank of the central sulcus was spared by this atrophy. Overlay with the JuBrain Cytoarchitectonic Atlas revealed this region to almost completely correspond to primary somatosensory area 3b. The other clusters of decreased cortical thickness in the left precentral (cluster size 3900.9 mm^2), postcentral (2547.7 mm^2), and superior frontal gyri (560.7 mm^2) as well as in the right precentral and postcentral gyri (5143.2 mm^2 and 4221.6 mm^2) attained the level of significance.

The cross-sectional comparison within ROIs defined by probability maps of cortical microstructure between baseline scans of patients with CBS and healthy controls revealed a pattern of atrophy similar to the whole-brain analysis (see Table 2). Bilaterally, patients with CBS had significantly smaller cortical thicknesses than controls in primary motor area 4, premotor area 6, and primary somatosensory cortical areas 1 and 2 ($p \leq 0.006$). In addition, significantly decreased cortical thicknesses were found in the right primary somatosensory area 3a ($p = 0.015$) of patients. No significant difference in cortical thickness in primary somatosensory area 3b was detected in either hemisphere. Subcortically, thalami, the putamina, and the nuclei accumbens of both hemispheres as well as the left amygdala and pallidum showed significantly smaller volumes in patients with CBS than healthy controls ($p \leq 0.026$). All other comparisons led to nonsignificant findings. Effect size analyses revealed medium to large effects for all significant differences found [Cohen's d (Cohen, 1992): range 0.53–1.67]. Supplemental Fig. 2 illustrates the distribution of individual morphometry results in patients and healthy controls.

3.2. Longitudinal changes

Linear mixed models revealed significant interactions of group and time in premotor area 6 and primary somatosensory areas 1, 3a, and 3b as well as the thalamus, putamen, and amygdala, with higher rates of atrophy in patients than controls ($p \leq 0.009$). Within patients, the atrophy rates of cortical ROIs defined by probability maps of cortical microstructure were compared with the rate of atrophy in area 3b. Significant interaction effects of region and time with area 3b as the reference region were found for premotor area 6 as well as for primary somatosensory areas 1 and 2, with a higher rate of atrophy in comparison to area 3b ($p \leq 0.001$). Individual atrophy rates are illustrated in Fig. 2, with details of all longitudinal statistics given in Supplemental Tables 1 and 2.

The subgroups of patients who did and did not complete follow-up visits did not differ regarding age (mean ± SD; patients without follow-up: 66.9 ± 8.2; patients with follow-up: 64.3 ± 6.7; t-test $p = 0.305$), disease duration (mean ± SD in months; patients

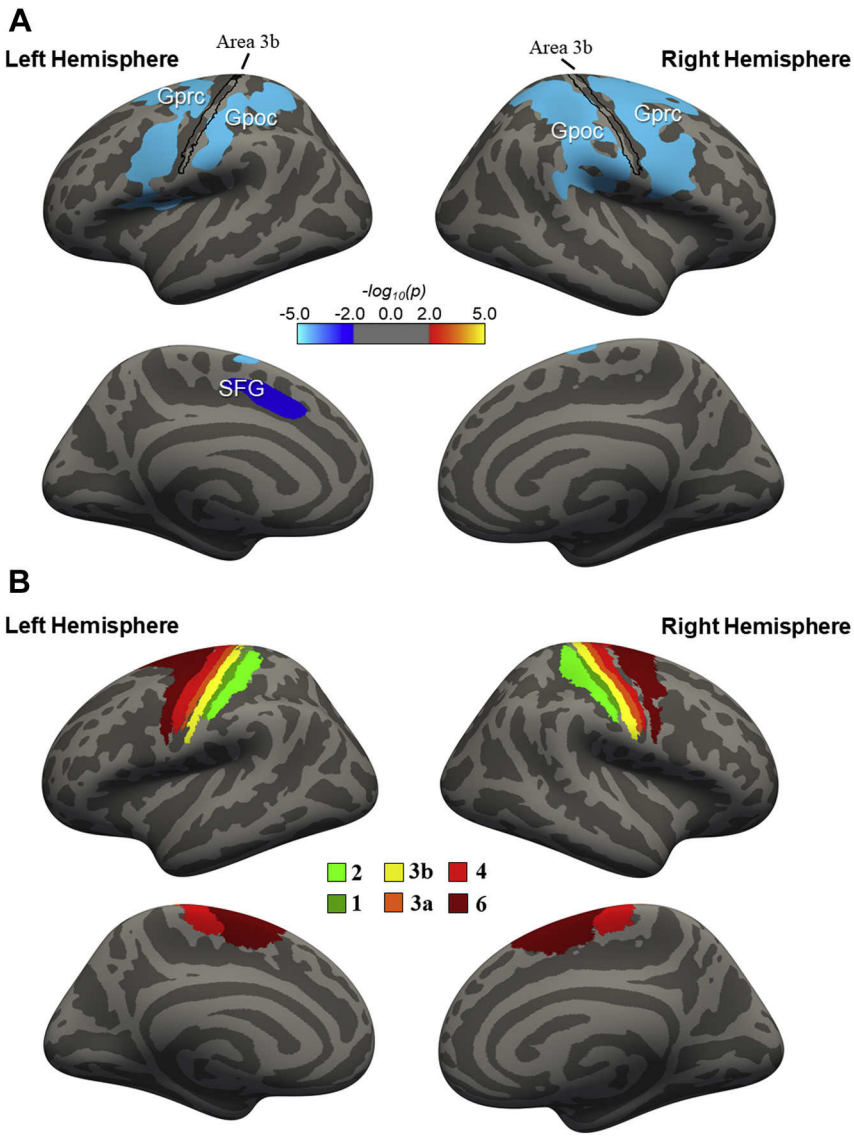

Fig. 1. Whole-brain surface-based comparison of cortical thickness between patients with CBS and healthy controls. (A) Clusters of significant differences in average cortical thickness between 36 baseline scans of patients with CBS and 24 baseline scans of healthy age- and gender-matched controls are presented. Whole-brain maps of cortical thicknesses were smoothed using the default FreeSurfer symmetric circular Gaussian kernel smoothing filter across the surface with a full width at half maximum (FWHM) of 10 mm. The Monte Carlo simulation was used to predict the distribution of the maximum cluster size under the null hypothesis (Hagler et al., 2006). The cluster size considered as significant was then corrected for multiple comparisons at $p < 0.01$. Significantly thinner cortices in patients were found in the precentral (Gprc) and postcentral (Gpoc) gyri of both hemispheres as well as in the superior frontal gyrus (SFG) of the left hemisphere. Remarkably, a region within the central sulcus corresponding to the probability map of microstructural area 3b was spared. (B) Probability maps to predict cytoarchitectonically defined areas along the central sulcus. Abbreviation: CBS, corticobasal syndrome.

without follow-up: 39.8 ± 30.6; patients with follow-up: 26.0 ± 11.7; *t*-test $p = 0.088$), or gender (female/male; patients without follow-up: 11/7; patients with follow-up: 14/4; chi-squared test $p = 0.278$) but differed regarding the baseline United Parkinson's Disease Rating Scale, whereby patients with a lower burden of motor symptoms were more likely to participate in the longitudinal study (mean ± SD; patients without follow-up: 37.1 ± 12.3; patients with follow-up: 23.4 ± 11.9; *t*-test $p = 0.003$).

3.3. Histological correlate of area-specific pericentral MRI findings

Tufted astrocytes were found predominantly in the precentral and the postcentral gyri. Most strikingly, the distribution of the tufted astrocytes was not homogeneous throughout but clearly followed areal boundaries of cytoarchitectonically defined brain regions: while there was considerable involvement of areas 4 and 6 of primary and premotor cortices as well as of areas 3a, 1, and 2 of the primary somatosensory cortex, primary somatosensory area 3b was almost completely spared. The affliction with tufted astrocytes ended abruptly at the cytoarchitectonic border between areas 3a and 3b as well as between areas 1 and 3b (Fig. 3). Additional regions affected by tufted astrocytes include secondary somatosensory and supplementary motor cortices, posterior-inferior frontal gyrus and prefrontal cortex, posterior-superior temporal gyrus, and an area within the dorsal aspect of the superior parietal lobe (see Fig. 3B and Supplementals, Fig. 3). The affliction with tufted astrocytes differed significantly between cytoarchitectonically defined areas (Welch-Test, $p < 0.001$, see Fig. 3). Post hoc tests with Tamhane's correction for heteroskedasticity revealed a significantly lower involvement in area 3b than in other primary somatosensory (areas 1, 2, and 3a) and motor areas (areas 4, 6; $p < 0.001$), while no significant difference between area 3b and the primary visual cortex as a control region

Table 2
Morphometry of cortical and subcortical regions in baseline scans of 36 patients with CBS and 24 healthy controls

Region	Side	CBS		Healthy controls		Difference		*p*-value		Effect size d
Cortical regions								Uncorrected	FDR corrected	
Area 1	**Left**	**2049.4**	**±39.1**	**2208.7**	**±36.0**	**−159.2**	**±56.2**	**0.006**	**0.011**	**0.75**
	Right	**1955.2**	**±45.0**	**2178.9**	**±40.4**	**−223.7**	**±64.3**	**0.001**	**0.002**	**0.92**
Area 2	**Left**	**1965.3**	**±28.6**	**2193.5**	**±31.2**	**−228.2**	**±43.4**	**<0.001**	**<0.001**	**1.39**
	Right	**1916.4**	**±40.2**	**2158.2**	**±23.6**	**−241.7**	**±46.6**[a]	**<0.001**[a]	**<0.001**	**1.37**
Area 3a	Left	1721.0	±18.1	1772.8	±24.3	−51.8	±29.7	0.087	0.112	0.46
	Right	**1713.0**	**±19.1**	**1789.7**	**±23.9**	**−76.6**	**±30.5**	**0.015**	**0.024**	**0.66**
Area 3b	Left	1578.6	±26.4	1592.6	±14.8	−14.0	±30.3[a]	0.645[a]	0.660	0.12
	Right	1557.2	±30.9	1604.0	±24.1	−46.8	±42.7	0.278	0.323	0.29
Area 4	**Left**	**2228.7**	**±36.2**	**2400.8**	**±36.2**	**−172.1**	**±55.8**	**0.003**	**0.007**	**0.79**
	Right	**2195.6**	**±37.2**	**2364.1**	**±45.7**	**−168.5**	**±58.9**	**0.006**	**0.011**	**0.53**
Area 6	**Left**	**2350.1**	**±34.3**	**2558.9**	**±31.3**	**−208.8**	**±49.2**	**<0.001**	**<0.001**	**1.12**
	Right	**2288.6**	**±38.9**	**2544.7**	**±34.4**	**−256.0**	**±55.3**	**<0.001**	**<0.001**	**1.22**
Subcortical regions										
Brainstem		19,318.8	±376.6	19,670.6	±556.4	−351.9	±647.0	0.089	0.112	0.46
Thalamus	**Left**	**6166.7**	**±147.5**	**6626.0**	**±183.3**	**−459.3**	**±234.6**	**0.003**	**0.007**	**0.82**
	Right	**6125.8**	**±127.3**	**6688.2**	**±182.5**	**−562.4**	**±215.6**	**<0.001**	**<0.001**	**1.04**
Amygdala	**Left**	**1400.5**	**±36.1**	**1538.7**	**±39.0**	**−138.2**	**±54.6**	**0.001**	**0.002**	**0.96**
	Right	1579.9	±41.4	1620.2	±40.8	−40.3	±60.7	0.087	0.112	0.46
Hippocampus	Left	3758.5	±65.8	3745.7	±59.5	+12.85	±94.1	0.318	0.350	0.27
	Right	3813.2	±79.8	3920.3	±79.3	−107.1	±116.3	0.047[a]	0.070	0.53
Pallidum	**Left**	**1744.2**	**±36.6**	**1914.4**	**±55.9**	**−170.1**	**±63.9**	**<0.001**	**0.001**	**1.00**
	Right	1753.4	±37.7	1778.4	±57.1	−25.0	±65.6	0.212	0.254	0.33
Putamen	**Left**	**3857.7**	**±85.8**	**4632.9**	**±134.3**	**−775.2**	**±151.8**	**<0.001**	**<0.001**	**1.49**
	Right	**3829.1**	**±92.3**	**4604.7**	**±110.3**	**−775.6**	**±144.6**	**<0.001**	**<0.001**	**1.67**
Ncl. caudatus	Left	3061.3	±88.2	3146.6	±73.6	−85.3	±123.7	0.115	0.141	0.42
	Right	3092.5	±87.5	3236.2	±86.2	−143.7	±128.3	0.037	0.057	0.56
Accumbens	**Left**	**372.7**	**±18.9**	**401.8**	**±12.3**	**−29.1**	**±19.8**	**0.026**[a]	**0.041**	**0.60**
	Right	**399.9**	**±12.9**	**450.2**	**±12.9**	**−50.3**	**±19.0**	**0.001**	**0.002**	**0.94**

Key: CBS, corticobasal syndrome; FDR, false discovery rate.
Mean ± standard error of the mean of the thickness (in μm, for cortical regions) and volume (in mm^3, for subcortical structures) of the baseline scans of 36 patients with CBS and 24 controls. Multiple t-tests were calculated for the comparison of average cortical thicknesses/volumes between baseline scans of patients and healthy controls. For t-tests of subcortical structures, volumes were normalized by the estimated total intracranial volume (ICV) to correct for differences in head size. FDR-corrected *p*-values < 0.05 were considered as statistically significant and presented in bold. The effect sizes were calculated with the web-based effect size calculator https://campbellcollaboration.org/research-resources/effect-size-calculator.html out of t and sample sizes.
[a] The assumption of equal variances was violated (Levene's test $p < 0.05$), and thus, corrected measures for the standard error of the mean difference and the resulting *p* value were used.

which is known to be not affected by CBS was found (V1; $p = 0.218$). All other areas showed a significantly higher burden of tufted astrocytes than the V1 ($p < 0.001$). The primary motor cortex (area 4) was more affected by tufted astrocytes than all other areas, with $p < 0.001$. Area 3a was less affected than area 1 ($p < 0.001$) and area 6 ($p = 0.012$). All other comparisons yielded findings of no significance.

The longitudinal change in the cortical thickness of the right hemisphere of the same patient measured in vivo over 26 months of disease progression showed a similar pattern of frontoparietal and particularly central atrophy as observed in the whole group (see previous Section 3) and as found in this patient histologically (see the last paragraph): area 3b was again spared, while there was pronounced atrophy in primary and premotor cortices as well as areas 3a, 1, and 2 of the primary somatosensory cortex (see Fig. 3D, right panel and 3C). This was accompanied by clusters of atrophy in the inferior frontal gyrus and superior and inferior temporal gyri.

Directly relating the histopathological disease burden, that is, tufted astrocytes, with the MRI-derived atrophy marker 'cortical thickness' revealed a significant association: a high tufted astrocyte load was related to local cortical thinning (Spearman's $\rho = -0.857$, $p = 0.014$).

4. Discussion

This multimodal and multilevel study found peculiar patterns of atrophy in patients with CBS, specifically localized to probability maps of distinct microstructurally defined functional brain areas. Our analyses consistently revealed that within the motor and somatosensory cortices, primary somatosensory area 3b was selectively less vulnerable to pathological processes, which was reflected cross-sectionally by nonmeasurable atrophy and longitudinally by slower atrophy rates of this area. The autopsy case of PSP-CBS resampled this atrophy pattern and provided a direct link between atrophy measured in vivo and histopathological changes detected postmortem. The data suggest that neurodegenerative processes in CBS selectively affect microstructurally defined regions and that these processes can be detected in the clinical setting via standard MRI-based measures.

4.1. Primary somatosensory area 3b is selectively less affected in CBS

The present study revealed that the tufted astrocytes in the individual autopsy case of PSP-CBS were not homogeneously distributed throughout the somatomotor cortex, as assumed before, but strictly followed boundaries of cytoarchitectonic brain regions (see Fig. 3). This finding is reflected in the pericentral atrophy observed cross-sectionally, which showed a selectively spared region on the caudal bank of the central sulcus (see Fig. 1). When assessing the pathological processes with respect to probability maps of microstructurally defined regions, cross-sectional ROI-based analyses showed a selectively unaffected primary somatosensory area 3b while the parietally adjacent somatosensory areas 1 and 2 as well as the frontally adjacent primary motor area 4 and premotor area 6 were clearly involved. Longitudinally, interaction effects of the group and time yielded significant results for somatosensory areas 1, 3a, and 3b as well as for premotor area 6, with declining cortical thicknesses over time in patients with CBS when

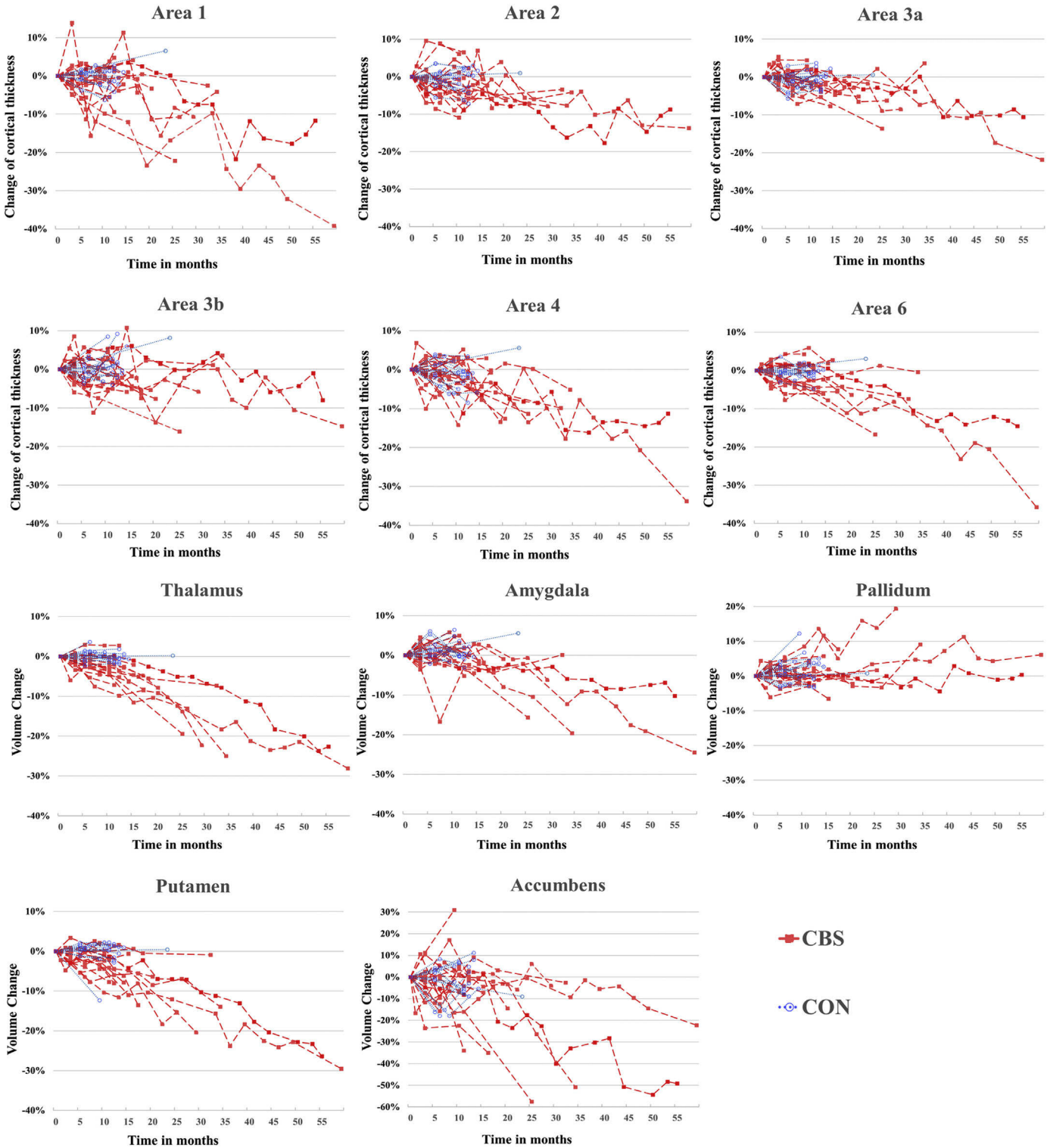

Fig. 2. Individual atrophy rates in patients with CBS and controls. Cortical thickness and subcortical volumes with significant atrophy when compared with healthy controls were longitudinally tracked within a subgroup of n = 18 patients with CBS (CON; red dashed lines, squares) and of n = 18 healthy matched controls (CON; blue dotted lines, circles). The percentage change at each time point regarding the baseline measurement (Baseline–Follow-up/Baseline) is shown. Abbreviation: CBS, corticobasal syndrome. (For interpretation of the references to color in this figure legend, the reader is referred to the Web version of this article.)

compared with healthy controls (see Supplemental Table 2). When comparing atrophy rates between cortical ROIs within patients with CBS, interaction effects of the region and time for somatosensory areas 1 and 2 as well as premotor area 6 showed significantly higher rates of atrophy than area 3b. The discrepancies between group*time and region*time interaction effects, especially regarding area 3b, indicate that atrophy may also occur in area 3b in later stages of the disease, albeit to a lesser extent than in other pericentral regions. Evidence for an affliction of primary somatosensory area 3a was mixed. Histological and longitudinal MRI

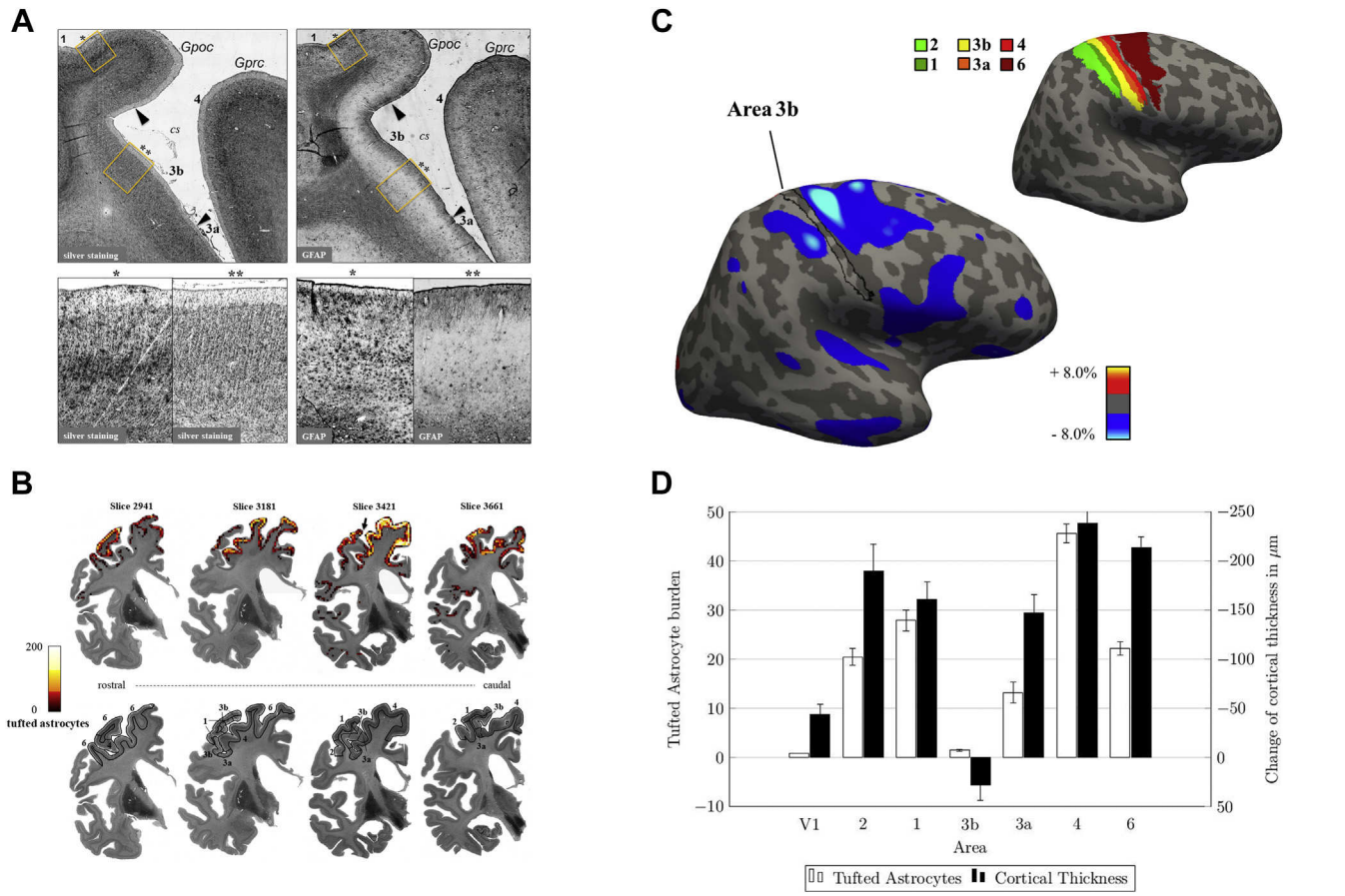

Fig. 3. Density of tufted astrocytes in the central region. (A) The distribution of tufted astrocytes was not homogenous but rather followed the sharp boundaries of the underlying cytoarchitectonically defined areas. A similar distribution of reactive astrocytes was seen on GFAP staining. (B) Tufted astrocytes were automatically quantified using a machine-based learning approach. Tiles with a tufted astrocyte count more than 10 (corresponding to the 90th percentile) are presented. An arrow marks the region in slice 3421 where the histologic images of in panel A have been extracted. (C) Thresholded spatial probability maps and voxel-wise percentage change of the right hemisphere after 26 months. For longitudinal processing, an individual unbiased template over time was created, and the rate of atrophy with respect to the temporal average thickness is given (for details of longitudinal processing, see Supplementals). Changes greater than ±4% are presented. (D) Comparative illustration of the tufted astrocyte burden and longitudinal change of cortical thickness of the right hemisphere of one patient with PSP-CBS in cytoarchitectonic areas of the primary somatosensory cortex (1, 2, 3a, and 3b), the primary motor cortex (4), the premotor cortex (6), and the primary visual cortex (V1). V1 served as a control region where no major changes were expected (Boxer et al., 2006; Dutt et al., 2016; Huey et al., 2009; Josephs et al., 2008; Südmeyer et al., 2012; Upadhyay et al., 2016). Error bars represent the standard error of the mean (for tufted astrocyte count) or the standard error of the difference (for cortical thickness). Abbreviations: CBS, corticobasal syndrome; CS, central sulcus; Gpoc, gyrus postcentralis; Gprc, gyrus precentralis; PSP, progressive supranuclear palsy.

analysis revealed a pronounced affliction of this area. However, the cross-sectional ROI-based analysis showed significant atrophy of area 3a only on the right hemisphere while the cross-sectional vertex-based analysis showed inconsistent atrophy within area 3a on both hemispheres.

Within the somatosensory cortex, area 3b serves as the core primary somatosensory cortex for tactile and area 3a for proprioceptive stimuli while the more associative areas 1 and 2 derive input from several cortico-cortical and subcortical connections (Hömke et al., 2009; Kaas, 2012). The clinical phenotype in CBS resamples this distinct affliction of areas within the somatosensory cortex, as the perception of primary tactile modalities is usually intact while integrative somatosensory functions as stereognosis or graphesthesia are frequently impaired (Levin et al., 2016; Mahapatra et al., 2004). The present study thus provides for the first time a multimodally determined correlate of these differential affections of somatosensory functions known and frequently observed in patients with CBS. Furthermore, it clearly argues in favor of dedicated structure-function relationships between microstructurally defined brain areas and specific functionalities.

In line with our study, an atrophy pattern spreading from the precentral gyrus to adjacent frontal regions covering the premotor cortex was consistently found in previous studies using cortical thickness analyses (McMillan et al., 2016; Upadhyay et al., 2016) and voxel-based estimations of local gray matter volume in clinically defined patients with CBS (Boxer et al., 2006; Huey et al., 2009) or autopsy-proven cases of CBD (Josephs et al., 2008; Lee et al., 2011; Whitwell et al., 2010). However, the pattern described here with a primary somatosensory area 3b that is selectively spared has not been described so far. In two studies comparing cortical thickness between patients and healthy controls, whole-cortex comparisons show a relatively unaffected region within the central sulcus, but the presumed association with the microstructurally defined area 3b was missed as morphometric changes were reported on the macro level regarding their locations in the lobes, gyri, or sulci (McMillan et al., 2016; Upadhyay et al., 2016). Our pathohistological data show a clear delineation between pathologically affected and unaffected brain tissue, which coincides with the border between the respective microstructural cortical areas. This suggests that the here used cytoarchitectonic atlas depicts neurodegenerative processes with higher precision relevant for understanding the

underlying pathogenetic mechanisms of the disease than other atlases. For example, macroanatomical atlases might obscure such effects as they aggregate the information of several microstructurally defined functional areas.

4.2. Implications for the pathogenesis of CBS

Possible explanations for a cortical spreading pattern that relies on cytoarchitectonically defined areas include (1) transmission of misfolded tau proteins along structural or functional connections or (2) different neurochemical environments. As CBS is usually seen in tauopathies such as CBD, PSP, or AD, this discussion will focus on hyperphosphorylated tau protein and its pathophysiologic mechanisms.

In a current concept of the pathophysiology of tauopathies, seeds of misfolded tau spread along transneuronal connections, and variations in these spreading patterns may account for the clinical heterogeneity of tauopathies (Braak and Del Tredici, 2018; Gibbons et al., 2018). For CBS, a frontoparietal spreading pattern is assumed (Ling et al., 2016; Tsuboi et al., 2005). However, a cell-to-cell transmission based on spatial proximity alone is not sufficient to explain the specific affliction of microstructurally defined cortical regions as found in our study. It has recently been shown that functional connections better predict tau spreading in AD than anatomical proximity (Franzmeier et al., 2019). The borders of microstructurally defined areas converge with borders of functional parcellations of the brain (Wig et al., 2014). In preclinical cases of CBD, an increased tau burden within the putamen was described, suggesting an early affliction during the disease (Ling et al., 2016). The putamen is embedded in corticobasal ganglia motor circuits and thus functionally connected with the primary motor cortex (Marchand et al., 2008; Miyachi et al., 2006). In line with this, in our study, significant cross-sectional and longitudinal putaminal atrophy was identified with an early and marked volume loss (see Fig. 2). Within the primary somatosensory cortex, connections of areas 2, 1, 3a, and 3b differ considerably, whereby area 3b almost exclusively receives input from thalamocortical projections, whereas the more associative areas 1 and 2 derive input from several cortico-cortical and subcortical connections (Hömke et al., 2009; Kaas, 2012). Variations in these projections between microstructurally defined somatosensory areas might provide a possible explanation for the marked differences in the pathological involvement of the somatosensory cortex but have not been particularly addressed in connectome studies so far.

In vitro and in vivo animal studies as well as postmortem studies have found that the occurrence of hyperphosphorylated tau varies with neurotransmitter concentrations or the density of receptor binding sites (Hellström-Lindahl, 2000; Pooler et al., 2013; Sasaki et al., 2009; Sindou et al., 1994; Yamada et al., 2014). Glutamatergic activity has been shown to facilitate the major steps in the development of tauopathies as tau hyperphosphorylation (Kobayashi et al., 2017; Sindou et al., 1994), its extracellular release (Kobayashi et al., 2017; Pooler et al., 2013; Yamada et al., 2014), and tau-related neurotoxicity (Crescenzi et al., 2017). In line, pharmacological antagonization of glutamatergic ionotropic *N*-methyl-D-aspartate (NMDA) or alpha-amino-3-hydroxy-5-methyl-4-isoxazolepropionic acid receptors or a reduced NMDA receptor expression have been shown to protect against tau hyperphosphorylation and tau-induced cell death (Amadoro et al., 2006; Kobayashi et al., 2017). The composition of transmitter receptors varies throughout the cortex and differs with its underlying cytoarchitecture, reflecting the distinct functional properties of different cortical areas (Caspers et al., 2015; Geyer et al., 1997; Toga et al., 2006; Zilles et al., 2002). Autoradiographic labeling studies described the specific compositions of neurochemical binding sites of each of the somatosensory areas [2, 1, 3b, and 3a (Geyer et al., 1997; Scheperjans et al., 2005)]. Area 3 b was especially characterized by a high density of serotonergic 5-HT2 binding sites and low density of L-glutamate binding sites as NMDA and alpha-amino-3-hydroxy-5-methyl-4-isoxazolepropionic acid receptors (Geyer et al., 1997; Scheperjans et al., 2005). Therefore, it is plausible to assume that glutamate-dependent neurotoxicity differs largely between cytoarchitectonic regions and thus provides a possible explanation for the sharp boundaries of atrophy and tufted astrocyte pathology found in the present study. It is worthy of note that the ligand-binding patterns of area 3a were similar but not the same as in area 3b, which may be reflected in the inconsistent finding of atrophy in area 3a in our study. However, glutamate is physiologically essential for neuronal plasticity, learning, and memory formation, and it remains unclear why a few individuals develop tauopathies while the majority does not (Niciu et al., 2012; Revett et al., 2013).

Taken together, an approach focusing on cytoarchitectonic rather than macroscopically defined regions when analyzing structural changes in CBS provides a better reflection of disease processes, as pathophysiologic mechanisms depend on characteristics which vary distinctly between cytoarchitectonic areas.

4.3. Cortical thickness as a biomarker for CBS clinical trials

The relevance of MR-based metrics in tauopathies was recently underlined by two studies showing that morphometric analyses more sensitively depict disease changes than tau-specific ^{18}F-AV-1451 PET in PSP (Whitwell et al., 2019) or CBS (Smith et al., 2017). This makes MR morphometry the preferable candidate as an objective biomarker, as it is also easier to apply in the general clinical patient population compared with PET. Despite the broad use of neuroimaging techniques in research and clinics, studies establishing direct associations between MRI atrophy and underlying pathohistological changes in neurodegenerative diseases are rare and merely rely on animal studies or qualitative descriptions (Paviour et al., 2004; Schocke et al., 2000). We could establish a direct link between tufted astrocytes and cortical thinning in a single case of PSP-CBS. This finding provides further support for the use of MR-based measures as a surrogate marker for underlying neuropathological processes, although the generalizability of this finding will have to be validated in further studies. Current disease-modifying interventional trials in CBS with anti-tau antibodies (NCT03658135), microtubule-stabilizing agents (NCT02133846), or autologous stem cell transplantation (NCT03297177) use structural MRI data as a secondary outcome parameter. However, the assessed targeted regions and follow-up periods differ widely. Our data suggest that ROIs defined by probability maps of microstructurally defined areas may describe neurodegenerative processes more accurately than macroanatomical region definitions. Based on microstructurally defined areas, we describe a distinct and multimodally robust pattern of atrophy and its dynamic over time, which may help in the specification of future study protocols.

4.4. Limitations

For our pathohistological data, a single case of PSP-CBS was examined. Therefore, conclusions regarding differences between neuropathological entities underlying CBS cannot be drawn. Lee et al compared patterns of atrophy in AD-CBS, PSP-CBS, and CBD-CBS and found pericentral neurodegeneration regardless of the underlying pathology (Lee et al., 2011). In our cohort of 36 CBS patients with presumably heterogeneous underlying neuropathologic entities, a pattern of pericentral atrophy comparable to the distribution of pathohistological processes in the case of PSP-CBS

was found, suggesting that similar pericentral neurodegenerative processes may be shared between CBS patients with differing neuropathological entities. However, we do not know the distribution of underlying neuropathologies in our sample. Thus, it remains unclear whether the heterogonous vulnerability of microstructural regions within the pericentral region found in our study applies to all underlying entities in the same way.

With follow-up times of up to five years, we provide the longest set of longitudinal morphometric data described in CBS so far. Nevertheless, our longitudinal data have rather heterogenous characteristics with a varying number of time points and follow-up times of between six months and five years. Therefore, our results might be biased toward those patients with longer follow-up times and more included time points. Moreover, patients with follow-ups showed a lower burden of motor symptoms as measured with the United Parkinson's Disease Rating Scale in comparison to patients who did not complete follow-up scans. Thus, the generalizability of our longitudinal results might primarily apply to patients in the early stages of their disease. These limitations, however, lay in the nature of longitudinal studies within such rapidly progressive and severely impairing disease. Nevertheless, they could provide relevant insight into a potentially vulnerable stage of disease which might help in further studying therapeutic intervention effects.

The assessment of somatosensory functions in our study was limited to routine clinical examinations. Future studies should include standardized measures of somatosensory functions to directly investigate the structure-function relationship of the heterogenous vulnerability for neurodegeneration within the primary somatosensory cortex found in our study.

5. Conclusion

We provide multimodal in vivo cross-sectional and longitudinal MRI and postmortem pathohistological evidence for a robust pattern of pericentral cortical atrophy in CBS covering the premotor, primary motor, and somatosensory cortical areas as well as the putamen. This pattern respects borders of microstructurally defined functional areas with a selectively less-affected primary somatosensory area 3b.

Disclosure statement

LD, MS, SR, TA, JF, SF, ASM, KA, and SC have nothing to declare. CJH received honoraria from Abbott. AS has received lecture fees from AbbVie, Boston Scientific, GlaxoSmithKline, MEDA Pharma, St Jude Medical, Medtronic, Teva Pharma, and UCB and served as a consultant for Boston Scientific, Grünenthal, Medtronic, and St Jude Medical.

CRediT authorship contribution statement

Lars Dinkelbach: Conceptualization, Data curation, Formal analysis, Investigation, Methodology, Project administration, Software, Visualization, Writing - original draft. **Martin Südmeyer:** Conceptualization, Writing - review & editing, Project administration, Funding acquisition, Supervision. **Christian Johannes Hartmann:** Investigation, Methodology, Writing - review & editing. **Sigrun Roeber:** Writing - review & editing, Investigation. **Thomas Arzberger:** Writing - review & editing, Investigation. **Jörg Felsberg:** Writing - review & editing, Investigation, Validation. **Stefano Ferrea:** Writing - review & editing, Investigation. **Alexia-Sabine Moldovan:** Writing - review & editing, Investigation. **Katrin Amunts:** Conceptualization, Writing - review & editing. **Alfons Schnitzler:** Conceptualization, Writing - review & editing, Supervision. **Svenja Caspers:** Conceptualization, Writing - review & editing, Funding acquisition, Methodology, Project administration, Resources, Validation, Supervision.

Acknowledgements

The authors thank all collaborating clinics and donors as well as patients' families who made this study possible. The authors gratefully acknowledge the time granted by the JARA-HPC Vergabegremium for computations on the supercomputer JURECA at Forschungszentrum Juelich. They also thank Peter Billard for his assistance with language editing.

The work received funding through the Initiative and Networking Fund of the Helmholtz Association (SC), and from the European Union's Horizon 2020 Research and Innovation Programme under Grant Agreement No. 785907 (HBP SGA2; KA and SC) and 945539 (HBP SGA3, KA and SC). The BrainNet Germany was supported by the Federal Ministry of Health (Bundesgesundheitsministerium).

Appendix A. Supplementary data

Supplementary data to this article can be found online at https://doi.org/10.1016/j.neurobiolaging.2020.05.009.

References

Alexander, S.K., Rittman, T., Xuereb, J.H., Bak, T.H., Hodges, J.R., Rowe, J.B., 2014. Validation of the new consensus criteria for the diagnosis of corticobasal degeneration. J. Neurol. Neurosurg. Psychiatry 85, 925–929.

Amadoro, G., Ciotti, M.T., Costanzi, M., Cestari, V., Calissano, P., Canu, N., 2006. NMDA receptor mediates tau-induced neurotoxicity by calpain and ERK/MAPK activation. Proc. Natl. Acad. Sci. 103, 2892–2897.

Amunts, K., Zilles, K., 2015. Architectonic mapping of the human brain beyond Brodmann. Neuron 88, 1086–1107.

Arganda-Carreras, I., Kaynig, V., Rueden, C., Eliceiri, K.W., Schindelin, J., Cardona, A., Sebastian Seung, H., 2017. Trainable Weka Segmentation: a machine learning tool for microscopy pixel classification. Bioinformatics 33, 2424–2426.

Armstrong, M.J., Litvan, I., Lang, A.E., Bak, T.H., Bhatia, K.P., Borroni, B., Boxer, A.L., Dickson, D.W., Grossman, M., Hallett, M., 2013. Criteria for the diagnosis of corticobasal degeneration. Neurology 80, 496–503.

Benjamini, Y., Hochberg, Y., 1995. Controlling the false discovery rate: a practical and powerful approach to multiple testing. J. R. Stat. Soc. Ser. B (Methodological) 57, 289–300.

Boeve, B.F., Lang, A.E., Litvan, I., 2003. Corticobasal degeneration and its relationship to progressive supranuclear palsy and frontotemporal dementia. Ann. Neurol. 54, S15–S19.

Boeve, B.F., Maraganore, D.M., Parisi, J.E., Ahlskog, J.E., Graff-Radford, N., Caselli, R.J., Dickson, D.W., Kokmen, E., Petersen, R.C., 1999. Pathologic heterogeneity in clinically diagnosed corticobasal degeneration. Neurology 53, 795.

Borroni, B., Garibotto, V., Agosti, C., Brambati, S.M., Bellelli, G., Gasparotti, R., Padovani, A., Perani, D., 2008. White matter changes in corticobasal degeneration syndrome and correlation with limb apraxia. Arch. Neurol. 65, 796–801.

Boxer, A.L., Geschwind, M.D., Belfor, N., Gorno-Tempini, M.L., Schauer, G.F., Miller, B.L., Weiner, M.W., Rosen, H.J., 2006. Patterns of brain atrophy that differentiate corticobasal degeneration syndrome from progressive supranuclear palsy. Arch. Neurol. 63, 81–86.

Braak, H., Del Tredici, K., 2018. Spreading of tau pathology in sporadic Alzheimer's disease along cortico-cortical top-down connections. Cereb. Cortex 28, 3372–3384.

Buckner, R.L., Head, D., Parker, J., Fotenos, A.F., Marcus, D., Morris, J.C., Snyder, A.Z., 2004. A unified approach for morphometric and functional data analysis in young, old, and demented adults using automated atlas-based head size normalization: reliability and validation against manual measurement of total intracranial volume. Neuroimage 23, 724–738.

Caspers, J., Palomero-Gallagher, N., Caspers, S., Schleicher, A., Amunts, K., Zilles, K., 2015. Receptor architecture of visual areas in the face and word-form recognition region of the posterior fusiform gyrus. Brain Struct. Funct. 220, 205–219.

Cohen, J., 1992. A power primer. Psychol. Bull. 112, 155–159.

Crescenzi, R., DeBrosse, C., Nanga, R.P., Byrne, M.D., Krishnamoorthy, G., D'aquilla, K., Nath, H., Morales, K.H., Iba, M., Hariharan, H., Lee, V.M.Y., Detre, J.A., Reddy, R., 2017. Longitudinal imaging reveals subhippocampal dynamics in glutamate levels associated with histopathologic events in a mouse model of tauopathy and healthy mice. Hippocampus 27, 285–302.

Dale, A.M., Fischl, B., Sereno, M.I., 1999. Cortical surface-based analysis: I. Segmentation and surface reconstruction. Neuroimage 9, 179–194.

de la Vega, A., Chang, L.J., Banich, M.T., Wager, T.D., Yarkoni, T., 2016. Large-scale meta-analysis of human medial frontal cortex reveals tripartite functional organization. J. Neurosci. 36, 6553–6562.
Dickson, D.W., Ahmed, Z., Algom, A.A., Tsuboi, Y., Josephs, K.A., 2010. Neuropathology of variants of progressive supranuclear palsy. Curr. Opin. Neurol. 23, 394–400.
Dutt, S., Binney, R.J., Heuer, H.W., Luong, P., Attygalle, S., Bhatt, P., Marx, G.A., Elofson, J., Tartaglia, M.C., Litvan, I., McGinnis, S.M., Dickerson, B.C., Kornak, J., Waltzman, D., Voltarelli, L., Schuff, N., Rabinovici, G.D., Kramer, J.H., Jack, C.R., Miller, B.L., Rosen, H.J., Boxer, A.L., 2016. Progression of brain atrophy in PSP and CBS over 6 months and 1 year. Neurology 87, 2016–2025.
Eickhoff, S.B., Heim, S., Zilles, K., Amunts, K., 2006. Testing anatomically specified hypotheses in functional imaging using cytoarchitectonic maps. Neuroimage 32, 570–582.
Eickhoff, S.B., Jbabdi, S., Caspers, S., Laird, A.R., Fox, P.T., Zilles, K., Behrens, T.E., 2010. Anatomical and functional connectivity of cytoarchitectonic areas within the human parietal operculum. J. Neurosci. 30, 6409–6421.
Fischl, B., Dale, A.M., 2000. Measuring the thickness of the human cerebral cortex from magnetic resonance images. Proc. Natl. Acad. Sci. 97, 11050–11055.
Franzmeier, N., Rubinski, A., Neitzel, J., Kim, Y., Damm, A., Na, D.L., Kim, H.J., Lyoo, C.H., Cho, H., Finsterwalder, S., Duering, M., Seo, S.W., Ewers, M., 2019. Functional connectivity associated with tau levels in ageing, Alzheimer's, and small vessel disease. Brain 142, 1093–1107.
Genon, S., Reid, A., Li, H., Fan, L., Müller, V.I., Cieslik, E.C., Hoffstaedter, F., Langner, R., Grefkes, C., Laird, A.R., Fox, P.T., Jiang, T., Amunts, K., Eickhoff, S.B., 2018. The heterogeneity of the left dorsal premotor cortex evidenced by multimodal connectivity-based parcellation and functional characterization. Neuroimage 170, 400–411.
Geyer, S., 2004. The microstructural border between the motor and the cognitive domain in the human cerebral cortex. Adv. Anat. Embryol. Cell Biol. 174. I-VIII, 1-89.
Geyer, S., Ledberg, A., Schleicher, A., Kinomura, S., Schormann, T., Bürgel, U., Klingberg, T., Larsson, J., Zilles, K., Roland, P.E., 1996. Two different areas within the primary motor cortex of man. Nature 382, 805–807.
Geyer, S., Schleicher, A., Zilles, K., 1997. The somatosensory cortex of human: cytoarchitecture and regional distributions of receptor-binding sites. Neuroimage 6, 27–45.
Geyer, S., Schleicher, A., Zilles, K., 1999. Areas 3a, 3b, and 1 of human primary somatosensory cortex: 1. Microstructural organization and interindividual variability. Neuroimage 10, 63–83.
Geyer, S., Schormann, T., Mohlberg, H., Zilles, K., 2000. Areas 3a, 3b, and 1 of human primary somatosensory cortex: 2. Spatial normalization to standard anatomical space. Neuroimage 11, 684–696.
Gibbons, G.S., Lee, V.M., Trojanowski, J.Q., 2018. Mechanisms of cell-to-cell transmission of pathological tau: a review. JAMA Neurol. 76, 101–108.
Goldenberg, G., 1995. Imitating gestures and manipulating a mannikin—the representation of the human body in ideomotor apraxia. Neuropsychologia 33, 63–72.
Goldenberg, G., 1996. Defective imitation of gestures in patients with damage in the left or right hemispheres. J. Neurol. Neurosurg. Psychiatry 61, 176–180.
Hagler Jr., D.J., Saygin, A.P., Sereno, M.I., 2006. Smoothing and cluster thresholding for cortical surface-based group analysis of fMRI data. Neuroimage 33, 1093–1103.
Hellström-Lindahl, E., 2000. Modulation of β-amyloid precursor protein processing and tau phosphorylation by acetylcholine receptors. Eur. J. Pharmacol. 393, 255–263.
Hömke, L., Amunts, K., Bönig, L., Fretz, C., Binkofski, F., Zilles, K., Weder, B., 2009. Analysis of lesions in patients with unilateral tactile agnosia using cytoarchitectonic probabilistic maps. Hum. Brain Mapp. 30, 1444–1456.
Huey, E.D., Pardini, M., Cavanagh, A., Wassermann, E.M., Kapogiannis, D., Spina, S., Ghetti, B., Grafman, J., 2009. Association of ideomotor apraxia with frontal gray matter volume loss in corticobasal syndrome. Arch. Neurol. 66, 1274–1280.
Iwamura, Y., Iriki, A., Tanaka, M., 1994. Bilateral hand representation in the postcentral somatosensory cortex. Nature 369, 554–556.
Iwasaki, Y., Yoshida, M., Hattori, M., Goto, A., Aiba, I., Hashizume, Y., Sobue, G., 2004. Distribution of tuft-shaped astrocytes in the cerebral cortex in progressive supranuclear palsy. Acta Neuropathol. 108, 399–405.
Josephs, K.A., Petersen, R.C., Knopman, D.S., Boeve, B.F., Whitwell, J.L., Duffy, J.R., Parisi, J.E., Dickson, D.W., 2006. Clinicopathologic analysis of frontotemporal and corticobasal degenerations and PSP. Neurology 66, 41–48.
Josephs, K.A., Whitwell, J.L., Dickson, D.W., Boeve, B.F., Knopman, D.S., Petersen, R.C., Parisi, J.E., Jack, C.R., 2008. Voxel-based morphometry in autopsy proven PSP and CBD. Neurobiol. Aging 29, 280–289.
Kaas, J.H., 2012. Somatosensory System The Human Nervous System, 3rd ed. Academic Press, London, United Kingdom, pp. 1074–1109.
Kertesz, A., McMonagle, P., Blair, M., Davidson, W., Munoz, D.G., 2005. The evolution and pathology of frontotemporal dementia. Brain 128, 1996–2005.
Kobayashi, S., Tanaka, T., Soeda, Y., Almeida, O.F., Takashima, A., 2017. Local somatodendritic translation and hyperphosphorylation of tau protein triggered by AMPA and NMDA receptor stimulation. EBioMedicine 20, 120–126.
Kouri, N., Whitwell, J.L., Josephs, K.A., Rademakers, R., Dickson, D.W., 2011. Corticobasal degeneration: a pathologically distinct 4R tauopathy. Nat. Rev. Neurol. 7, 263–272.
Lee, S.E., Rabinovici, G.D., Mayo, M.C., Wilson, S.M., Seeley, W.W., DeArmond, S.J., Huang, E.J., Trojanowski, J.Q., Growdon, M.E., Jang, J.Y., Sidhu, M., See, T.M., Karydas, A.M., Gorno-Tempini, M.-L., Boxer, A.L., Weiner, M.W., Geschwind, M.D., Rankin, K.P., Miller, B.L., 2011. Clinicopathological correlations in corticobasal degeneration. Ann. Neurol. 70, 327–340.
Levin, J., Kurz, A., Arzberger, T., Giese, A., Höglinger, G.U., 2016. The differential diagnosis and treatment of atypical parkinsonism. Dtsch. Arztebl. Int. 113, 61–69.
Ling, H., Kovacs, G.G., Vonsattel, J.P.G., Davey, K., Mok, K.Y., Hardy, J., Morris, H.R., Warner, T.T., Holton, J.L., Revesz, T., 2016. Astrogliopathy predominates the earliest stage of corticobasal degeneration pathology. Brain. 139, 3237–3252.
Ling, H., O'Sullivan, S.S., Holton, J.L., Revesz, T., Massey, L.A., Williams, D.R., Paviour, D.C., Lees, A.J., 2010. Does corticobasal degeneration exist? A clinicopathological re-evaluation. Brain 133, 2045–2057.
Mahapatra, R.K., Edwards, M.J., Schott, J.M., Bhatia, K.P., 2004. Corticobasal degeneration. Lancet Neurol. 3, 736–743.
Marchand, W.R., Lee, J.N., Thatcher, J.W., Hsu, E.W., Rashkin, E., Suchy, Y., Chelune, G., Starr, J., Barbera, S.S., 2008. Putamen coactivation during motor task execution. Neuroreport 19, 957–960.
McMillan, C.T., Boyd, C., Gross, R.G., Weinstein, J., Firn, K., Toledo, J.B., Rascovsky, K., Shaw, L., Wolk, D.A., Irwin, D.J., Lee, E.B., Trojanowski, J.Q., Grossman, M., 2016. Multimodal imaging evidence of pathology-mediated disease distribution in corticobasal syndrome. Neurology 87, 1227–1234.
Merker, B., 1983. Silver staining of cell bodies by means of physical development. J. Neurosci. Methods 9, 235–241.
Merzenich, M.M., Kaas, J.H., Sur, M., Lin, C.S., 1978. Double representation of the body surface within cytoarchitectonic area 3b and 1 in "SI" in the owl monkey (Aotus trivirgatus). J. Comp. Neurol. 181, 41–73.
Miyachi, S., Lu, X., Imanishi, M., Sawada, K., Nambu, A., Takada, M., 2006. Somatotopically arranged inputs from putamen and subthalamic nucleus to primary motor cortex. Neurosci. Res. 56, 300–308.
Niciu, M.J., Kelmendi, B., Sanacora, G., 2012. Overview of glutamatergic neurotransmission in the nervous system. Pharmacol. Biochem. Behav. 100, 656–664.
Ouchi, H., Toyoshima, Y., Tada, M., Oyake, M., Aida, I., Tomita, I., Satoh, A., Tsujihata, M., Takahashi, H., Nishizawa, M., Shimohata, T., 2014. Pathology and sensitivity of current clinical criteria in corticobasal syndrome. Mov. Disord. 29, 238–244.
Paviour, D., Schott, J., Stevens, J., Revesz, T., Holton, J., Rossor, M., Lees, A., Fox, N., 2004. Pathological substrate for regional distribution of increased atrophy rates in progressive supranuclear palsy. J. Neurol. Neurosurg. Psychiatry 75, 1772–1775.
Pooler, A.M., Phillips, E.C., Lau, D.H., Noble, W., Hanger, D.P., 2013. Physiological release of endogenous tau is stimulated by neuronal activity. EMBO Rep. 14, 389–394.
Rebeiz, J.J., Kolodny, E.H., Richardson, E.P., 1968. Corticodentatonigral degeneration with neuronal achromasia. Arch. Neurol. 18, 20–33.
Reuter, M., Schmansky, N.J., Rosas, H.D., Fischl, B., 2012. Within-subject template estimation for unbiased longitudinal image analysis. Neuroimage 61, 1402–1418.
Revett, T.J., Baker, G.B., Jhamandas, J., Kar, S., 2013. Glutamate system, amyloid β peptides and tau protein: functional interrelationships and relevance to Alzheimer disease pathology. J. Psychiatry Neurosci. 38, 6–23.
Sasaki, K., Shimura, H., Itaya, M., Tanaka, R., Mori, H., Mizuno, Y., Kosik, K.S., Tanaka, S., Hattori, N., 2009. Excitatory amino acid transporter 2 associates with phosphorylated tau and is localized in neurofibrillary tangles of tauopathic brains. FEBS Lett. 583, 2194–2200.
Scheperjans, F., Grefkes, C., Palomero-Gallagher, N., Schleicher, A., Zilles, K., 2005. Subdivisions of human parietal area 5 revealed by quantitative receptor autoradiography: a parietal region between motor, somatosensory, and cingulate cortical areas. Neuroimage 25, 975–992.
Schmitz, T.W., Spreng, R.N., Weiner, M.W., Aisen, P., Petersen, R., Jack, C.R., Jagust, W., Trojanowki, J.Q., Toga, A.W., Beckett, L., 2016. Basal forebrain degeneration precedes and predicts the cortical spread of Alzheimer's pathology. Nat. Commun. 7, 13249.
Schocke, M.F., Waldner, R., Puschban, Z., Kolbitsch, C., Seppi, K., Scherfler, C., Kremser, C., Zschiegner, F., Felber, S., Poewe, W., Wenning, G.K., 2000. In vivo magnetic resonance imaging of embryonic neural grafts in a rat model of striatonigral degeneration (multiple system atrophy). Neuroimage 12, 209–218.
Sindou, P., Lesort, M., Couratier, P., Yardin, C., Esclaire, F., Hugon, J., 1994. Glutamate increases tau phosphorylation in primary neuronal cultures from fetal rat cerebral cortex. Brain Res. 646, 124–128.
Smith, R., Schöll, M., Widner, H., van Westen, D., Svenningsson, P., Hägerström, D., Ohlsson, T., Jögi, J., Nilsson, C., Hansson, O., 2017. In vivo retention of 18F-AV-1451 in corticobasal syndrome. Neurology 89, 845–853.
Spina, S., Brown, J.A., Deng, J., Gardner, R.C., Nana, A.L., Hwang, J.-H.L., Gaus, S.E., Huang, E.J., Kramer, J.H., Rosen, H.J., Kornak, J., Neuhaus, J., Miller, B.L., Grinberg, L.T., Boxer, A.L., Seeley, W.W., 2019. Neuropathological correlates of structural and functional imaging biomarkers in 4-repeat tauopathies. Brain 142, 2068–2081.
Südmeyer, M., Pieperhoff, P., Ferrea, S., Krause, H., Groiss, S.J., Elben, S., Wojtecki, L., Zilles, K., Amunts, K., Schnitzler, A., 2012. Longitudinal deformation-based morphometry reveals spatio-temporal dynamics of brain volume changes in patients with corticobasal syndrome. PLoS one 7, e41873.
Toga, A.W., Thompson, P.M., Mori, S., Amunts, K., Zilles, K., 2006. Towards multimodal atlases of the human brain. Nat. Rev. Neurosci. 7, 952–966.

Togo, T., Dickson, D.W., 2002. Tau accumulation in astrocytes in progressive supranuclear palsy is a degenerative rather than a reactive process. Acta Neuropathol. 104, 398–402.

Tsuboi, Y., Josephs, K.A., Boeve, B.F., Litvan, I., Caselli, R.J., Caviness, J.N., Uitti, R.J., Bott, A.D., Dickson, D.W., 2005. Increased tau burden in the cortices of progressive supranuclear palsy presenting with corticobasal syndrome. Mov. Disord. 20, 982–988.

Upadhyay, N., Suppa, A., Piattella, M.C., Di Stasio, F., Petsas, N., Colonnese, C., Colosimo, C., Berardelli, A., Pantano, P., 2016. Gray and white matter structural changes in corticobasal syndrome. Neurobiol. Aging 37, 82–90.

Wang, Z., Xia, M., Dai, Z., Liang, X., Song, H., He, Y., Li, K., 2015. Differentially disrupted functional connectivity of the subregions of the inferior parietal lobule in Alzheimer's disease. Brain Struct. Funct. 220, 745–762.

Whitwell, J.L., Jack, C.R., Boeve, B.F., Parisi, J.E., Ahlskog, J.E., Drubach, D.A., Senjem, M.L., Knopman, D.S., Petersen, R.C., Dickson, D.W., Josephs, K.A., 2010. Imaging correlates of pathology in corticobasal syndrome. Neurology 75, 1879–1887.

Whitwell, J.L., Tosakulwong, N., Schwarz, C.G., Botha, H., Senjem, M.L., Spychalla, A.J., Ahlskog, J.E., Knopman, D.S., Petersen, R.C., Jack Jr., C.R., Lowe, V.J., Josephs, K.A., 2019. MRI Outperforms [18F] AV-1451 PET as a longitudinal biomarker in progressive supranuclear palsy. Mov. Disord. 34, 105–113.

Wig, G.S., Laumann, T.O., Petersen, S.E., 2014. An approach for parcellating human cortical areas using resting-state correlations. Neuroimage 93, 276–291.

Yamada, K., Holth, J.K., Liao, F., Stewart, F.R., Mahan, T.E., Jiang, H., Cirrito, J.R., Patel, T.K., Hochgräfe, K., Mandelkow, E.-M., Holtzman, D.M., 2014. Neuronal activity regulates extracellular tau in vivo. J. Exp. Med. 211, 387–393.

Zilles, K., Amunts, K., 2010. Centenary of Brodmann's map—conception and fate. Nat. Rev. Neurosci. 11, 139–145.

Zilles, K., Palomero-Gallagher, N., Grefkes, C., Scheperjans, F., Boy, C., Amunts, K., Schleicher, A., 2002. Architectonics of the human cerebral cortex and transmitter receptor fingerprints: reconciling functional neuroanatomy and neurochemistry. Eur. Neuropsychopharmacol. 12, 587–599.